scientific reports

Check for updates

OPEN

M2 microglia-derived exosomes reduce neuronal ferroptosis via FUNDC1-mediated mitophagy by activating AMPK/ULK1 signaling

Jian Li[1], Qing Chen[1] & Hao Gu[2]✉

Neuronal ferroptosis plays a vital role in the progression of neonatal hypoxic-ischemic brain damage (HIBD). M2-type microglia-derived exosomes (M2-exos) have been shown to protect neurons from ischemia–reperfusion (I/R) brain injury, but their impact on I/R-induced neuronal ferroptosis and the underlying mechanisms remain poorly understood. In this study, we used an in vitro oxygen-glucose deprivation/reoxygenation (OGD/R) model in HT-22 neuronal cells to investigate how M2-exos modulate ferroptosis. We found that M2-exos were internalized by HT-22 cells and significantly attenuated OGD/R-induced ferroptosis. Mechanistically, M2-exos enhanced mitophagy, which was mediated by the upregulation of FUN14 domain-containing protein 1 (FUNDC1), thereby inhibiting ferroptosis. Further analysis revealed that M2-exos activated FUNDC1-dependent mitophagy through the AMP-activated protein kinase (AMPK)/UNC-51-like kinase 1 (ULK1) signaling pathway. Taken together, these findings suggest that M2-exos ameliorate I/R-induced neuronal ferroptosis by enhancing FUNDC1-mediated mitophagy through the activation of AMPK/ULK1 signaling pathway.

Keywords Microglia, Exosome, Ferroptosis, Mitophagy, Ischemia/reperfusion

Abbreviations

M2-exos	M2-type microglia-derived exosomes
HIBD	Neonatal hypoxic-ischemic brain damage
I/R	Ischemia/reperfusion
OGD/R	Oxygen-glucose deprivation/reoxygenation
FUNDC1	FUN14 domain-containing protein 1
AMPK	AMP-activated protein kinase
ULK1	UNC-52-like kinase 1
HIE	Hypoxic-ischemic encephalopathy

Neuronal ferroptosis refers to the death of neurons caused by the accumulation of excess iron ions in cells[1]. In hypoxic-ischemic encephalopathy (HIE), neuronal ferroptosis may be one of the important pathological processes[2–4]. HIE is brain damage caused by neonates suffering from hypoxia and/or ischemia during the perinatal period[5]. In this case, the balance of intracellular iron ions may be disrupted due to insufficient oxygen supply and metabolic disorders[6]. Excess iron ions can cause oxidative stress and intracellular damage, leading to neuronal death. Excessive iron ions can cause neuronal death through multiple pathways, including promoting oxidative stress, damaging mitochondrial function, and triggering apoptosis[6]. These processes may aggravate the neurological damage of HIE and have a negative impact on the long-term neurological function of children. Therefore, intervention targeting neuronal ferroptosis may become a potential strategy to alleviate neurological damage in HIE.

Microglia play an important role in HIE as they can participate in inflammatory responses and repair processes when the nervous system is damaged[7–9]. M2-type microglia are a specific type of microglia often associated with anti-inflammatory and repair processes[9]. Previous studies have shown that during HIE, M2-type

[1]Department of Anesthesiology, The Affiliated Huaian No. 1 People's Hospital of Nanjing Medical University, No. 1 the Yellow River West Road, Huaiyin District, Huai'an City 223300, Jiangsu Province, China. [2]Department of Pediatrics, The Affiliated Huaian No. 1 People's Hospital of Nanjing Medical University, No. 1 the Yellow River West Road, Huaiyin District, Huai'an City 223300, Jiangsu Province, China. [3]Jian Li and·Qing Chen contributed equally. ✉email: ghghgh1115@126.com

microglia increase and release anti-inflammatory factors and neurotrophic factors, thereby reducing neuron damage and promoting nerve repair[9,10]. In addition, M2-type microglia also regulate inflammatory responses and reduce inflammatory damage to nerve cells[9,10]. Therefore, exploring the role of M2-type microglia in HIE is crucial to understand the pathophysiological mechanisms of this disease and to find potential therapeutic strategies. By promoting the activation and function of M2-type microglia, it may help reduce the neurological damage caused by HIE and improve the prognosis of children.

Neuronal ferroptosis and M2-type microglia may be related in some neurological diseases[11,12], but our understanding of their interactions in HIE is currently relatively limited. M2-type microglia have been shown to exert its function by secreting exosomes[13,14]. Exosomes are extracellular vesicles containing a lipid bilayer that contain various bioactive molecules such as proteins, nucleic acids, and lipids[15,16]. These exosomes are released outside cells through the in vitro secretion pathway, which can transmit information between cells and regulate physiological and pathological processes of cells[15,16]. Some studies have found that exosomes secreted by M2-type microglia contain a variety of bioactive molecules, such as anti-inflammatory factors, neurotrophic factors, and growth factors, which promotes the survival and functional recovery of neurons[15]. Further study may help reveal the mechanism of exosomes secreted by M2-type microglia in HIE and provide new ideas for the development of related therapeutic strategies.

The present study was aimed to investigate the effect of M2-type microglia derived exosomes (M2-exos) on neuronal ferroptosis and its potential mechanisms in vitro using an oxygen-glucose deprivation/reperfusion (OGD/R) model in HT-22 cells.

Materials and methods

Cell culture and treatment

BV-2 mouse microglial cell line and mouse hippocampal neuronal line (HT-22) were purchased from Shanghai Zhong Qiao Xin Zhou Co., Ltd. (Shanghai, China). BV-2 cells were cultured in MEM medium supplemented with 10% fetal bovine serum, 100 U/mL penicillin, and 100 U/mL streptomycin. HT-22 cells were cultured in DMEM complete medium. All cells were incubated in a humidified atmosphere of 5% CO_2 at 37 °C.

For M2-type microglial induction, BV2 cells were cultured in a medium containing recombinant protein IL-4 at 20 ng/mL for 48 h, and identified via western blot by detecting positive biomarkers (Arg1 and CD206). The oxygen-glucose deprivation and re-oxygenation (OGD/R) model was established in HT-22 neuron cell lines as previously reported[17,18]. Briefly, HT-22 cells were cultured in glucose-free DMEM and then transferred to a sealed hypoxic box containing a mixture of 95% N_2 and 5% CO_2 at 37 °C for 4 h. Thereafter, the cells were cultured in normal DMEM with 10% FBS and maintained for 24 h in reoxygenation under normoxic conditions. Model success was verified by ≥ 40% cell death (CCK-8 assay), 2-fold Fe^{2+} release increase, and GPX4 downregulation (Western blot), consistent with OGD/R-induced ferroptosis[19,20]. HT-22 cells cultured in growth culture medium under normoxic conditions served as a control. Conditioned medium (CM) from M2-type BV-2 cells were collected under sterile conditions followed by centrifugation at 3000*g* at 4 °C for 10 min to remove cells and then diluted to 1:1 with DMEM complete medium for further use. CM from normal cultured BV-2 cells was used as the control CM.

Cell viability assay

The viability of HT-22 cells was evaluated using the Cell Counting Kit-8 (CCK-8, MCE, Shanghai, China) assay. Briefly, HT-22 cells were seeded into 96-well plates at a density of 3×10^3 cells/well and then treated as described in the text. Subsequently, 20 μl CCK-8 was added to each well. After 2 h of incubation, the absorbance was measured using a plate reader (ELx800, BioTek Instruments, Inc., Vermont, USA) at 450 nm (A450). Cell viability was calculated as cell viability = OD (treatments)/OD (controls) × 100%.

MDA, SOD and iron content determination

The levels of MDA, GSH and iron in HT-22 cells were detected by an MDA assay kit (Jiancheng Bioengineering Institute, China), GSH assay kit (Jiancheng Bioengineering Institute, China), and intracellular Iron colorimetric assay kit (PPLYGEN, China), according to the manufacturer's instructions.

Western blotting

Western blotting assays were performed as previously described by us[21,22]. Briefly, a total of 25 ug proteins were separated using 4–12% SDS-PAGE gels and transferred onto PVDF membranes. The membranes were blocked with 5% skim milk at room temperature for 1 h, incubated with primary antibodies against CD63 (1:1000), TSG101 (1:1000), Arg1 (1:1000), CD206 (1:1000), SLC7A11, GPX4 (1:1000), TOMM20 (1:2000), TIMM23 (1:2000), LC3-II (1:2000), Phospho-AMPK(1:1000), AMPK(1:2000), Phospho-ULK1 (1:1000), ULK1 (1:2000), Phospho-FUNDC1 (1:1000), FUNDC1(1:2000), NCOA4 (1:2000) and β-actin (1:5000) at 4 °C overnight, followed by corresponding secondary antibodies. All primary and secondary antibodies were obtained from Biodragon (Suzhou, China). Blots were developed by ECL detection reagents (PECL08, Proteinbio, China).

Exosome isolation, characterization, labeling and treatment

Exosomes were purified from the cell culture supernatants of M2-type BV-2 cells using an ExoQuick exosome precipitation solution (System Bioscience, USA) according to the manufacturer's instructions. Briefly, M2-type BV-2 were cultured for 24 h in exosome-free MEM medium. The medium was then collected and centrifugated at 70,000×*g* overnight. The supernatant was then collected and further centrifuged for 1 h at 70,000×*g*. The exosome-containing pellet was washed with PBS, followed by centrifuged at 70,000×*g* for 1 h and resuspended in 200 µL of PBS. The exosomes were stored at −80 °C immediately after isolation until further analysis.

A transmission electron microscopy (JEM-1230, JEOL Ltd., Akishima, Japan) was used to identify the characteristic of the exosomes. Nanoparticle tracking analysis (NTA, Brookhaven, New York) was used to measure the diameter of exosomes. The protein content was measured using BCA protein assay, and exosome markers, CD63 and tumor susceptibility gene 101 (TSG101) were detected by western blot analysis.

For exosomal labeling, exosomes were labeled using PKH26 (cat. MIDI26, Sigma-Aldrich, Saint Louis, USA) following the manufacturer's procedures. Exosomes were incubated with PKH26 for 5 min. The reaction was then stopped with FBS. After washing with medium, PKH26-labeled exosomes (40 μg/mL) were added to HT-22 cells and incubated at 37 °C for 24 h. The cells were then incubated with DAPI (cat. 0100 - 20, Southern Biotech, Birmingham, USA) to stain the nuclei and observed via a fluorescence microscope (DM2500, Leica, Wetzlar, Germany).

For exosome treatment, after being cultured in oxygen-glucose deprivation (OGD) for 4 h, HT-22 cells were treated with fresh normal DMEM with 10% FBS containing 40 μg/mL exosome and placed back in a 5% CO_2 incubator for 24 h. PBS incubation was set as the control.

Immunofluorescence assay

HT-22 cells were seeded onto cover glasses in 6-well plates and treated as described in the text. After washing twice with PBS, MitoTracker Red CMXRos probe (200 nM, Beyotime, China) was added and the cells were incubated for another 30 min at 37 °C. Cells were fixed with 4% paraformaldehyde for 20 min, followed by permeabilization with 0.1% Triton-X 100 for 5 min. The cover glasses were then blocked with 1% bovine serum albumin (BSA) for 1 h and incubated with anti-LC3-II antibody at 4 °C overnight. Then, the cells were incubated with FITC-conjugated secondary antibodies (Invitrogen, Carlsbad, CA, USA) for 1 h and stained with 4′,6-diamidino-2-phenylindole (DAPI) for 10 min. Finally, images were collected using a fluorescent microscope (Leica DM2500, Wetzlar, Germany).

Statistical analysis

Data are expressed as mean ± standard deviation (SD) from a minimum of three independent experiments. All statistical analyses were conducted using Prism 10.0 software (GraphPad Software, USA). Prior to analysis, data were assessed for normality (Shapiro-Wilk test) and homogeneity of variance (Levene's test). For datasets satisfying these assumptions, comparisons between two groups were performed using Student's *t*-test, while multiple-group comparisons were analyzed by ordinary one-way ANOVA along with Tukey's post hoc test. For datasets violating normality or homogeneity assumptions, non-parametric tests were applied. A p-value < 0.05 was considered statistically significant. Despite the absence of dedicated funding, this study utilized established protocols and shared laboratory resources to ensure reproducibility. Sample sizes were determined based on pilot effect sizes and prior literature.

Results

M2-type BV-2 attenuated OGD/R-induced ferroptosis in HT-22 cells by secreting exosomes

We first investigated the effect of M2-type microglia on neuronal ferroptosis, BV-2 cells were first polarized to the M2 type by IL-4. The mRNA levels of M2-type markers CD206 and Arg1 were increased after IL-4 induction (Fig. 1A). Western blot and immunofluorescence analysis also showed that IL-4 stimulation significantly upregulated the protein levels of CD206 and Arg1 (Fig. 1B, C). As shown in Fig. 1D, compared with OGD/R alone, M2-conditioned medium (CM) significantly increased the viability of HT-22 cells subjected to OGD/R. The MDA levels were significantly higher in the OGD/R group than in the control group (Fig. 1E), and GSH levels in the OGD/R group was decreased compared with the control group (Fig. 1F). In contrast, CM could reduce MDA levels and increase GSH levels in OGD/R-exposed HT-22 cells (Fig. 1E-F). Moreover, CM could reduce iron content in OGD/R-exposed HT-22 cells (Fig. 1G). Western blot analysis showed that OGD/R significantly increased NCOA4 expression, and decreased the expression of SLC7A11 and GPX4 in HT-22 cells, which was attenuated by the addition of CM (Fig. 1H). To investigate the mechanism by which M2-type microglia ameliorated OGD/R-induced neuronal ferroptosis, the exosome inhibitor GW4869 was added into the CM. The result showed that CM increased the viability in OGD/R-exposed HT-22 cells, which was inhibited by GW4869 (Fig. 1D). GW4869 also attenuated CM-induced increases in GSH and iron levels and decreases in MDA levels (Fig. 1E–G). The decreased NCOA4 levels, increased SLC7A11 and GPX4 levels induced by CM were also reversed by GW4869 (Fig. 1H). These results suggested that M2-type microglia attenuated OGD/R-induced neuronal ferroptosis by secreting exosomes.

Isolation and identification of exosomes derived from M2-type BV2 cells

To investigate the potential roles of exosomes derived from M2-type BV2 cells (M2-exos) in OGD/R-induced neuronal ferroptosis, M2-exos were first isolated (Fig. 2A) and verified with transmission electron microscopy (TEM), western blot, and nanoparticle tracking analysis (NTA). The TEM results revealed that M2-exos exhibited round-shaped morphology, which is consistent with the typical exosomal morphology (Fig. 2B). NTA data indicated that the diameters of the M2-exos were mostly approximately 70 nm (Fig. 2C). Western blot results confirmed the presence of specific exosome surface markers (TSG101, and CD63) and absence of cell-specific markers (GM130 and Calnexin) in M2-exos (Fig. 2D). Collectively, these results confirmed that the M2-exos were successfully isolated and identified.

M2-exos attenuated OGD/R-induced ferroptosis of HT-22 cells

To investigate the effect of M2-exos on OGD/R-induced ferroptosis, HT-22 cells were cultured in OGD conditions for 4 h and then cocultured with M2-exos in the 24 h reperfusion phase. As shown in Fig. 3A, M2-exos increased the viability of HT-22 in a concentration-dependent manner under OGD/R conditions.

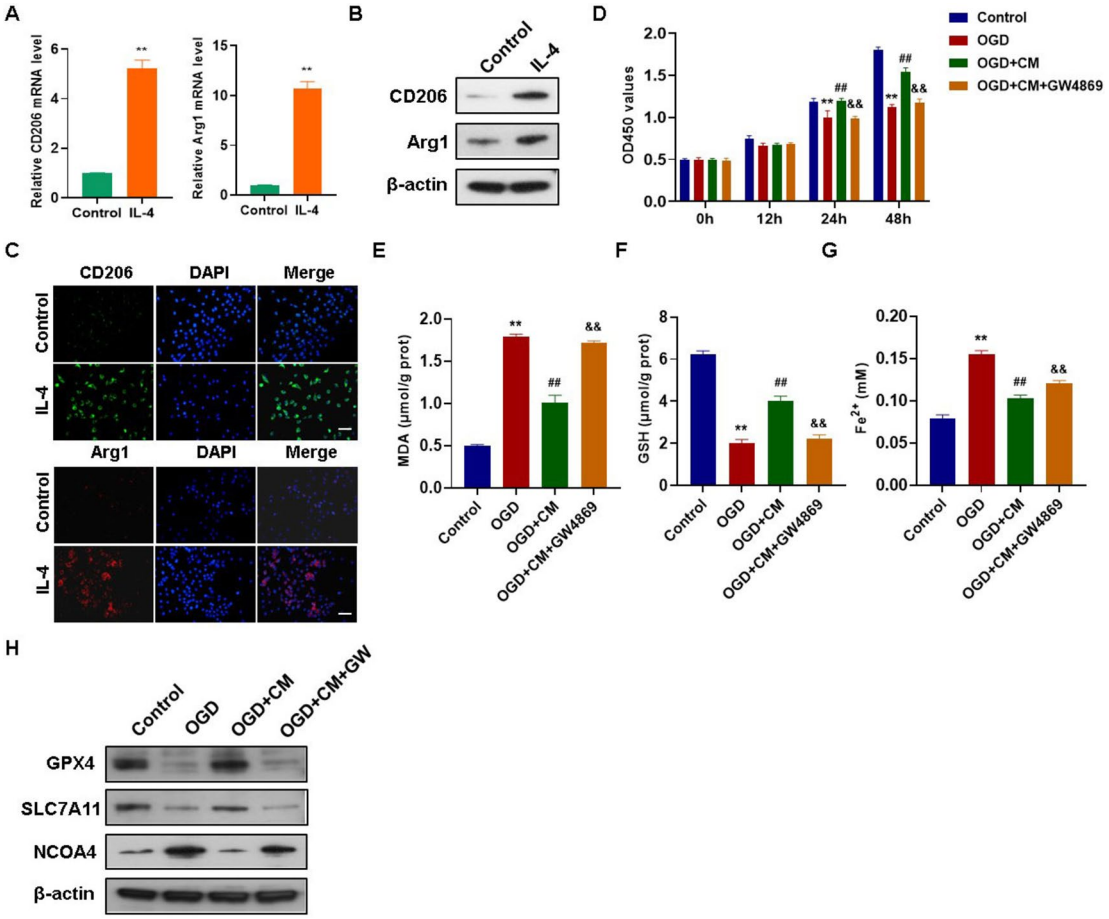

Fig. 1. Effects of M2-type BV-2 conditioned medium and the exosome inhibitor GW4869 on OGD/R-induced ferroptosis in HT-22 cells. (**A**–**C**) BV-2 cells were treated with 20 ng/ml IL-4 for 48 h, and the expression levels of CD206 and Arg1 were detected by RT-qPCR, western blot, and immunofluorescence, respectively. Scar bar = 100 μm. (**D**–**H**) HT-22 cells were cultured under normal conditions (control), or underwent OGD/R treatment (OGD), or pretreated with M2-BV2-conditioned medium (CM) and exposed to OGD/R treatment (OGD + CM), or pretreated with CM plus GW4869 and exposed to OGD/R treatment (OGD + CM + GW4869). The viability of HT-22 cells in each group was detected by CCK-8 assay (**D**), the MDA, GSH and iron levels in each group were detected by specific kit, respectively (**E**–**G**), and the expression levels of SLC7A11, GPX4 and NCOA4 in each group were detected by western blot (**H**). $^{**}p < 0.01$ compared with control group; $^{\#\#}p < 0.01$ compared with OGD group; $^{\&\&}p < 0.01$ compared with OGD + CM group.

As no comparable improved effects on the viability of HT-22 cells were observed at concentrations of 40 μg/mL and 80 μg/mL (Fig. 3A), the concentration of 40 μg/mL was selected to conduct subsequent experiments. Immunofluorescence results showed PKH26-labeled M2-exos (40 μg/mL) in HT-22 cells, indicating successful uptake of M2-exos (Fig. 3B). OGD/R increased MDA and iron levels and NCOA4 expression, decreased the GSH levels and the protein expression levels of SLC7A11 and GPX4 in HT-22 cells (Fig. 3C–F). In contrast, M2-exos treatment partly abolished these effects of OGD/R exposure (Fig. 3C–F). Collectively, these data suggested that M2-exos attenuated OGD/R-induced ferroptosis of HT-22 cells.

M2-exos attenuated OGD/R-induced ferroptosis of HT-22 cells by enhancing mitophagy

Previous studies demonstrated that inhibition of mitophagy contributes to neuronal ferroptosis[23,24]. Thus, we wondered whether mitophagy is involved in the protective effect of M2-exos against OGD/R-induced neuronal ferroptosis. As shown in Fig. 4A, M2-exos-induced mitophagy was demonstrated by co-localization between mitochondria and the autophagosome marker LC3B-II. Western blot analysis showed that M2-exos reduced TIMM23 and TOMM20 levels, and increased LC3B-II level in OGD/R-exposed cells (Fig. 4B). When mitophagy was suppressed with a mitophagy inhibitor (mitochondrial division inhibitor-1, Mdivi-1) or an autophagy inhibitor (3-methyladenine, 3-MA) in OGD/R-exposed HT-22 cells treated with M2-exos, the viability of HT-22 cells was significantly decreased (Fig. 4C), the level of GSH was significantly decreased (Fig. 4D), the levels of MDA and iron were significantly increased (Fig. 4E, F), the protein expression levels of NCOA4 were increased, and the protein expression levels of SLC7A11 and GPX4 were significantly decreased (Fig. 4G). Collectively, these findings suggest that M2-exos attenuated OGD/R-induced ferroptosis of HT-22 cells by enhancing mitophagy.

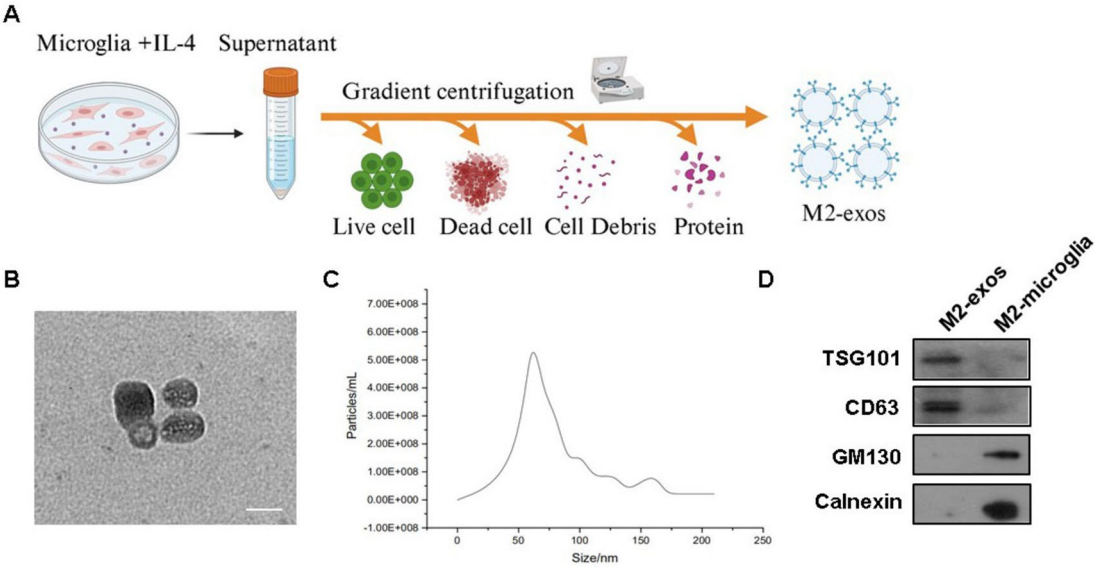

Fig. 2. Identification of exosomes derived from M2-type BV2 cells (M2-exos). (**A**) Flow chart of acquisition of exosomes from M2-type BV2 cells. (**B**) Exosomes were observed under a transmission electron microscope. Scale bar: 200 nm. (**C**) The size of exosomes was assessed by nanoparticle tracking analysis (NTA). (**D**) Expression levels of exosomal markers (TSG101, and CD63) and cell-specific markers (GM130 and Calnexin) were measured by western blotting.

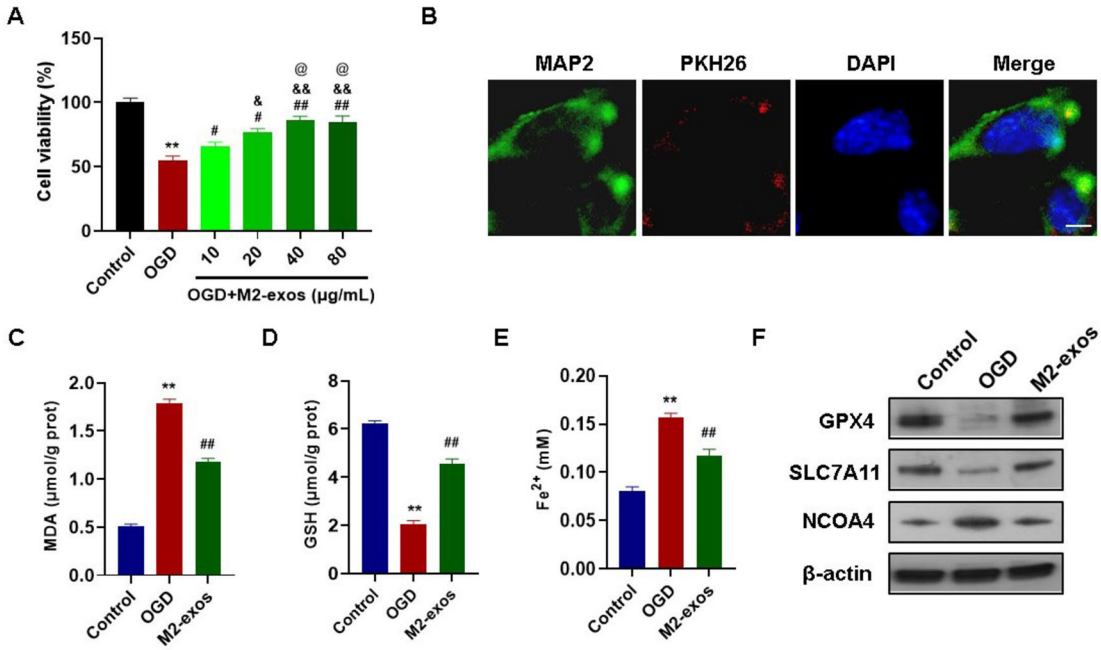

Fig. 3. Effect of M2-exos on OGD/R-induced ferroptosis of HT-22 cells. (**A**) HT-22 cells were cultured under three different conditions: normal (control), OGD/R (OGD), and OGD/R with different concentrations of M2-exos. After 24 h of culture, cell viability was determined by the CCK-8 assay. (**B**) MSC-exos are internalized by HT-22 cells. PKH26-labeled M2-exos are shown in red, MAP2-labeled HT-22 cells are shown in green, and DAPI-labeled nuclei are shown in blue. Scale bar: 50 μm. (**C**–**F**) HT-22 cells were cultured under three conditions: normal (control), OGD/R (OGD), and OGD/R + 40 μg/mL MSC-exos (M2-exos). After 24 h of culture, the MDA, GSH and iron levels in each group were detected by specific kit, respectively (**C**–**E**), and the expression levels of SLC7A11, GPX4 and NCOA4 in each group were detected by western blot (**F**). $^{**}p < 0.01$ compared with control group; $^{\#}p < 0.05$, $^{\#\#}p < 0.01$ compared with OGD group; $^{\&}p < 0.05$, $^{\&\&}p < 0.01$ compared with OGD + M2-exos (10 μg/mL) group; $^{@}p < 0.05$ compared with OGD + M2-exos (20 μg/mL) group.

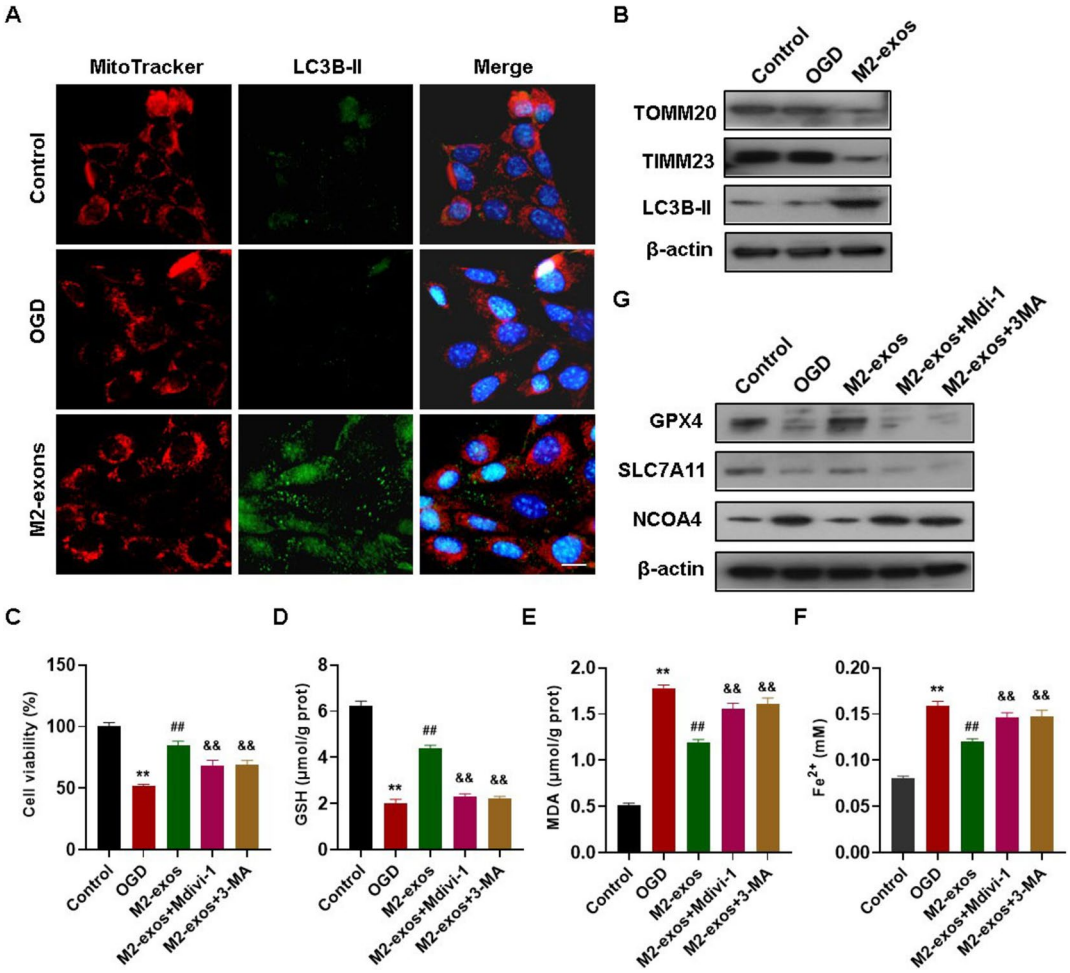

Fig. 4. Mitophagy is required for the protective effect of M2-exos against OGD/R-induced ferroptosis of HT-22 cells. (**A**, **B**) HT-22 cells were cultured under three conditions: normal (control), OGD/R (OGD), and OGD/*R* + 40 μg/mL M2-exos (M2-exos). After 24 h of culture, (**A**) The cells were stained with MitoTracker Red followed by immunostaining with LC3B-II antibody. Scale bar: 50 μm. (**B**) the expression levels of TIMM23, TOMM20 and LC3B-II were detected by western blot. (**C**–**G**) HT-22 cells were treated as follows: normal (control), OGD/R (OGD), OGD/R + M2-exos treatment (M2-exos), pretreated with vehicle (Vech), 3-methyladenine (3MA, 10 mM), or mitochondrial division inhibitor-1 (Mdi-1, 10 μM) followed by M2-exos treatment. After 24 h of treatment, (**C**) cell viability was determined by the CCK-8 assay. (**D**–**F**) the MDA, GSH and iron levels in each group were detected by specific kit, respectively. (**G**) The expression levels of SLC7A11, GPX4 and NCOA4 in each group were detected by western blot. $^{**}p < 0.01$ compared with control group; $^{\#}p < 0.05$, $^{\#\#}p < 0.01$ compared with OGD group; $^{\&}p < 0.05$, $^{\&\&}p < 0.01$ compared with M2-exos group.

M2-exos activated FUNDC1-mediated mitophagy via AMPK/ULK1 to ameliorate OGD/R-induced ferroptosis of HT-22

FUN14 domain-containing protein 1 (FUNDC1)-mediated mitophagy has been shown to exert protective effects against cerebral ischemia-reperfusion (IR) injury[12,25,26]. Moreover, the AMPK–ULK1 pathway has been shown to activate FUNDC1 to promote mitophagy[27,28]. Therefore, we next investigated the involvement of AMPK/ULK1/FUNDC1 axis in M2-exos-induced mitophagy in our system. The results showed significant decreases in the phosphorylation levels of AMPK, ULK1 and FUNDC1 under OGD/R conditions (Fig. 5A). M2-exos treatment significantly increased the phosphorylation levels of these proteins in OGD/R-exposed HT-22 cells (Fig. 5A). Furthermore, dorsomorphin (AMPK inhibitor) and SBI-0206965(ULK1 inhibitor) significantly reduced the phosphorylation levels of FUNDC1 in M2-exo-treated HT-22 cells under OGD/R conditions (Fig. 5A). Dorsomorphin and SBI-0206965 also significantly inhibited M2-exos-induced downregulation of TIMM23 and TOMM20 levels, and upregulation of LC3B-II in OGD/R-exposed HT-22 cells (Fig. 5A). Furthermore, the M2-exos-induced increases in cell viability (Fig. 5B), GSH level (Fig. 5C), and expression levels of SLC7A11 and GPX4 (Fig. 5A), and decreases in MDA (Fig. 5D), iron levels (Fig. 5E) and expression levels of NCOA4 (Fig. 5A) were significantly reversed by drsomorphin and SBI-0206965 treatment. Collectively, these results indicated that M2-exos exerted its protective effect against ferroptosis by activating FUNDC1-dependent mitophagy through the AMPK/ULK1 pathway.

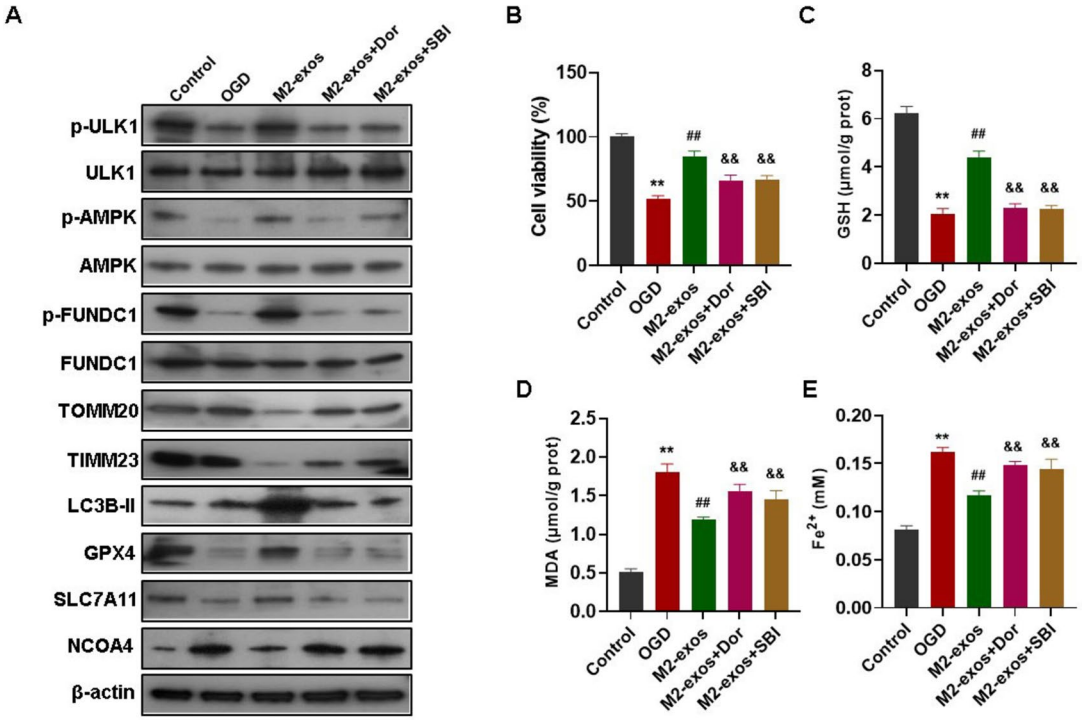

Fig. 5. The AMPK/ULK1/FUNDC1 signaling pathway is required for the M2-exos-induced mitophagy and inhibition ferroptosis in OGD/R-exposed HT-22 cells. HT-22 cells were cultured under the conditions: normal (control), OGD/R (OGD), OGD/*R* + 40 μg/mL M2-exos (M2-exos), pretreated with Dorsomorphin (Dor, 10 mM), or SBI-0206965 (SBI, 10 μM) followed by M2-exos treatment. After 24 h of treatment, the expression levels of p-AMPK, AMPK, p-ULK1, ULK1, p-FUNDC1, FUNDC1, TIMM23, TOMM20, LC3B-II, SLC7A11, GPX4 and NCOA4 were detected by western blot (**A**), cell viability was determined by the CCK-8 assay (**B**), the MDA, GSH and iron levels in each group were detected by specific kit, respectively (**C**–E). $^{**}p < 0.01$ compared with control group; $^{\#}p < 0.05$, $^{\#\#}p < 0.01$ compared with OGD group; $^{\&}p < 0.05$, $^{\&\&}p < 0.01$ compared with M2-exos group.

Discussion

Neuronal ferroptosis has been demonstrated to play a critical role in the progression of neonatal HIBD[2,29]. Additionally, previous studies revealed that exosomes-derived from different types of cells exerted protective effects against ferroptosis in various cells[30–32]. In the present study, we found that M2-exos significantly increased cell viability and the expression levels of the key proteins associated with ferroptosis, and reduced the levels of MDA and iron in OGD/R-exposed HT-22 cells. These findings suggested that M2-exos exerted protective effects against I/R-induced neuronal ferroptosis. Our results are consistent with a previous study reported by Xie et al.[33]. They also found that exosomes derived from M2-type microglia could ameliorate OGD/R-induced injury by inhibiting ferroptosis in HT-22 cells[33]. While Xie's and our studies demonstrate the protective effects of M2-exo against OGD/R-induced injury in TH-22 cells, several limitations must be acknowledged, particularly regarding the acute-phase experimental design. Firstly, our findings are based on acute-phase assessments, which may not fully capture the long-term therapeutic potential or possible delayed adverse effects of M2-exos. Secondly, the TH-22 cell line, while useful for mechanistic studies, does not fully replicate the complexity of in vivo neuronal networks, glial interactions, or systemic inflammatory responses. The absence of blood-brain barrier dynamics, immune cell crosstalk, and vascular components may limit the translational relevance of our findings. Thirdly, the efficacy of M2-exos in in vitro OGD/R models does not guarantee similar outcomes in in vivo HIBD models, where factors like biodistribution, immune clearance, and off-target effects come into play. Preclinical validation in animal models is essential.

The mechanism by which M2-exos attenuate I/R-induced neuronal ferroptosis was then investigated. Mitophagy is a process that cells selectively wrap and degrade damaged mitochondria through an autophagy mechanism, thus maintaining mitochondria and intracellular homeostasis[34,35]. Mitophagy has been demonstrated to be involved in the pathogenesis of many clinical diseases and the regulation of mitophagy may become a new direction for the treatment of some diseases[34–36]. Recently, activation of mitophagy has been demonstrated to be a critical protective mechanism of exosomes against different diseases[12,24,37]. Importantly, mitophagy has been shown to suppress neuronal ferroptosis in some brain injury diseases[24,38]. In accordance with these results, the present study showed that M2-exos treatment significantly increased the levels of mitophagy in OGD/R-exposed HT-22 cells. When mitophagy was blocked with 3-MA or Mdivi-1, the protective effect of M2-exos against OGD/R-induced ferroptosis was markedly reversed in HT-22 cells. These data strongly indicated that M2-exos prevent OGD/R-induced ferroptosis of neuronal HT-22 cells by enhancing mitophagy. Recent studies, such as

Wang et al.[39], have highlighted the anti-ferroptotic potential of M2 microglia-derived exosomes in ischemic injury. Our study extends these findings by demonstrating that naturally secreted M2-exos mitigate neuronal ferroptosis through FUNDC1-dependent mitophagy, activated via the AMPK/ULK1 pathway, a mechanism not previously reported.

We next explored the potential activators for M2-exos-induced mitophagy in OGD/R-exposed HT-22 cells. FUNDC1 is an outer mitochondrial membrane (OMM) protein that acts as an autophagy receptor for mitophagy under hypoxic conditions[40]. Increasing evidence has indicated that FUNDC1-mediated mitophagy plays a critical role in inhibition of ferroptosis[41,42]. In this study, we found that M2-exos significantly increased the activity of FUNDC1 in OGD/R-exposed HT-22 cells, suggesting that M2-exos attenuated OGD/R-induced ferroptosis through FUNDC1-mediated mitophagy. AMPK has been identified as an indispensable inducer of FUNDC1-dependent mitophagy[40,43]. Reduced energy production increases AMP levels and thus promotes the phosphorylation of AMPK, which directly activates ULK1 by phosphorylating it at Ser317 or Ser777[40,43]. Upon its activation, ULK1 translocates to the mitochondrial outer membrane surface to phosphorylate FUNDC1 at Ser17, thus inducing mitophagy[40,43]. The AMPK/ULK1/FUNDC1 pathway-mediated mitophagy has been characterized as a protective mechanism under various pathological conditions, including cognitive impairment and myocardial fibrosis[28,39]. In the present study, we found that inhibition of AMPK or ULK1 activation significantly attenuated M2-exos-induced FUND1-dependent mitophagy and ferroptosis inhibition in OGD/R-exposed HT-22 cells, suggesting that M2-exos activates AMPK/ULK1/FUNDC1 pathway to enhance mitophagy to suppress OGD/R-induced ferroptosis in HT-22 cells.

It is well known that mitophagy is activated by two distinct pathways, one is ubiquitin dependent while the other is receptor dependent. The ubiquitin dependent pathway involves Parkin/PINK1 pathway-mediated ubiquitination. PINK1 accumulates at the outer membrane of dysfunctional mitochondria and recruits Parkin. Activated Parkin subsequently leads to the ubiquitination of substrates and the recruitment of autophagy receptors to initiate mitophagy[40,43]. In the receptor-dependent pathway, mitochondrial receptors like FUNDC1, BNIP3 and NIX, directly bind to LC3 or GABARAP to initiate mitophagy[40,43]. In addition to receptor dependent pathway, AMPK was also been shown to activate mitophagy through the Parkin/PINK1 pathway[40,44,45]. Whether the Parkin/PINK1 pathway is involved in AMPK-mediated mitophagy in our system is an interesting point for us to investigate in the near future.

M2-exos have been shown to exert their function by transferring proteins, messenger RNAs, and non-coding RNA to recipient cells[46,47]. Jiang et al. showed that the glioblastoma-associated M2-type microglia (GAM) could promote the angiogenesis of glioblastoma multiforme (GBM) via transporting exosomal circular RNA KIF18A (circKIF18A) into human brain microvessel endothelial cells (hBMECs)[47]. Liu et al. recently found that microglia-derived exosomes paraquat-induced neuronal damage by transferring circZNRF1[46]. Recent research has provided evidence that specific circRNA has the ability to modulate disease progression through diverse mechanisms, one of which is by regulating cellular ferroptosis. Importantly, the abnormal expression of circRNAs has been shown to be involved in the pathogenesis of neonatal HIBD[48,49]. Therefore, it is worthwhile to investigate which circRNA in M2-exos alleviates I/R-induced neuronal ferroptosis by activating FUNDC1-mediated mitophagy through the AMPK/ULK1 pathway.

Conclusion

In conclusion, our findings indicated that M2-exos alleviated I/R-induced neuronal ferroptosis by enhancing FUNDC1-mediated mitophagy via activating the AMPK/ULK1 pathway (Fig. 6). The findings in the present study provide a neuronal ferroptosis-centric view of the neuroprotective effect of M2-exos. These results demonstrated that M2-exos may be a promising target for the treatment of neonatal HIBD. While our study delineates the mechanistic role of M2-exos in vitro, future work will validate these findings in vivo using HIBD models to assess long-term neuroprotection and functional recovery. The unfunded nature of this work may limit the scale of certain analyses. However, the consistent mechanistic data across replicates support the conclusions.

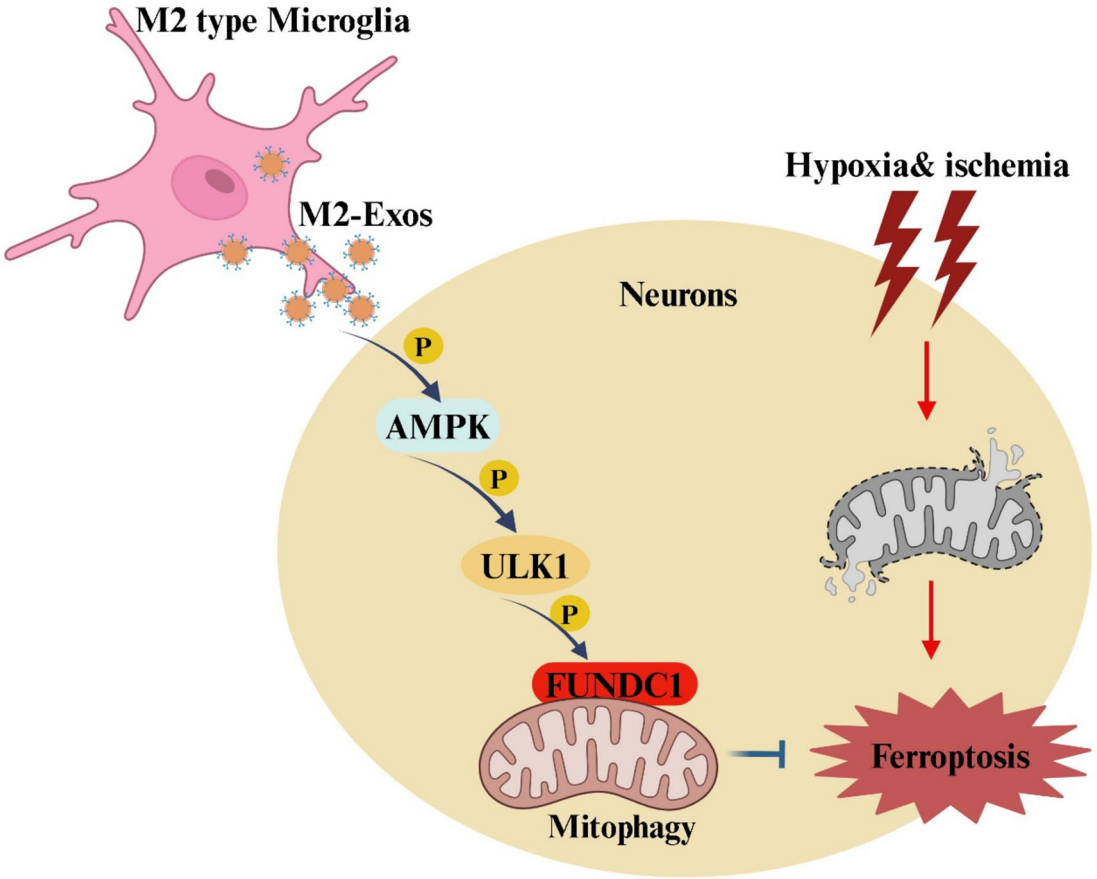

Fig. 6. A proposed model of M2-exos-induced mitophagy alleviates I/R-induced ferroptosis in neurons.

Data availability

The datasets used during the present study are available from the corresponding author upon reasonable request.

Received: 20 February 2025; Accepted: 19 May 2025
Published online: 23 May 2025

References

1. Jacquemyn, J., Ralhan, I. & Ioannou, M. S. Driving factors of neuronal ferroptosis. *Trends Cell. Biol.* **34** (7), 535–546. https://doi.org/10.1016/j.tcb.2024.01.010 (2024). Epub 2024/02/24. PubMed PMID: 38395733.
2. Lin, J. et al. Catalpol alleviates hypoxia ischemia-induced brain damage by inhibiting ferroptosis through the PI3K/NRF2/system Xc-/GPX4 axis in neonatal rats. *Eur. J. Pharmacol.* **968**, 176406. https://doi.org/10.1016/j.ejphar.2024.176406 (2024). Epub 2024/02/11. PubMed PMID: 38341076.
3. Zhu, K. et al. Inhibition of TLR4 prevents hippocampal hypoxic-ischemic injury by regulating ferroptosis in neonatal rats. *Exp. Neurol.* **345**, 113828. https://doi.org/10.1016/j.expneurol.2021.113828 (2021). Epub 2021/08/04. PubMed PMID: 34343528.
4. Tan, X. et al. Iron overload facilitates neonatal hypoxic-ischemic brain damage via SLC7A11-mediated ferroptosis. *J. Neurosci. Res.* **101** (7), 1107–1124. https://doi.org/10.1002/jnr.25184 (2023). Epub 2023/03/18. PubMed PMID: 36929608.
5. Victor, S., Rocha-Ferreira, E., Rahim, A., Hagberg, H. & Edwards, D. New possibilities for neuroprotection in neonatal hypoxic-ischemic encephalopathy. *Eur. J. Pediatr.* **181** (3), 875–887. https://doi.org/10.1007/s00431-021-04320-8 (2022). Epub 2021/11/26. PubMed PMID: 34820702; PubMed Central PMCID: PMCPMC8897336.
6. Hu, X. et al. Emerging role of STING signalling in CNS injury: inflammation, autophagy, necroptosis, ferroptosis and pyroptosis. *J. Neuroinflammation*. **19** (1), 242. https://doi.org/10.1186/s12974-022-02602-y (2022). Epub 2022/10/05. PubMed PMID: 36195926; PubMed Central PMCID: PMCPMC9531511.
7. Li, B., Dasgupta, C., Huang, L., Meng, X. & Zhang, L. MiRNA-210 induces microglial activation and regulates microglia-mediated neuroinflammation in neonatal hypoxic-ischemic encephalopathy. *Cell. Mol. Immunol.* **17** (9), 976–991. https://doi.org/10.1038/s41423-019-0257-6 (2020). Epub 2019/07/14. PubMed PMID: 31300734; PubMed Central PMCID: PMCPMC7608107.
8. Chen, H. R. et al. Monocytes promote acute neuroinflammation and become pathological microglia in neonatal hypoxic-ischemic brain injury. *Theranostics* **12** (2), 512–529. https://doi.org/10.7150/thno.64033 (2022). Epub 2022/01/04. PubMed PMID: 34976198; PubMed Central PMCID: PMCPMC8692901.
9. Bregere, C., Schwendele, B., Radanovic, B. & Guzman, R. Microglia and stem-tell mediated neuroprotection after neonatal hypoxia-Ischemia. *Stem Cell. Rev. Rep.* **18** (2), 474–522. https://doi.org/10.1007/s12015-021-10213-y (2022). Epub 2021/08/13. PubMed PMID: 34382141; PubMed Central PMCID: PMCPMC8930888.
10. Yu, L. et al. Atorvastatin promotes Pro/anti-inflammatory phenotypic transformation of microglia via Wnt/beta-catenin pathway in Hypoxic-Ischemic neonatal rats. *Mol. Neurobiol.* **61** (6), 3559–3577. https://doi.org/10.1007/s12035-023-03777-y (2024). Epub 2023/11/24. PubMed PMID: 37996729; PubMed Central PMCID: PMCPMC11087325.

11. Gao, Y. et al. Annexin A5 ameliorates traumatic brain injury-induced neuroinflammation and neuronal ferroptosis by modulating the NF-kB/HMGB1 and Nrf2/HO-1 pathways. *Int. Immunopharmacol.* **114**, 109619. https://doi.org/10.1016/j.intimp.2022.109619 (2023). Epub 2023/01/27.
12. Chen, D. et al. FUNDC1-induced mitophagy protects spinal cord neurons against ischemic injury. *Cell. Death Discov.* **10** (1), 4. https://doi.org/10.1038/s41420-023-01780-9 (2024). Epub 2024/01/05.
13. Song, Y. et al. M2 microglia-derived exosomes protect the mouse brain from ischemia-reperfusion injury via Exosomal miR-124. *Theranostics* **9** (10), 2910–2923. https://doi.org/10.7150/thno.30879 (2019). Epub 2019/06/28.
14. Guan, P. et al. M2 microglia-derived exosome-loaded electroconductive hydrogel for enhancing neurological recovery after spinal cord injury. *J. Nanobiotechnol.* **22** (1), 8. https://doi.org/10.1186/s12951-023-02255-w (2024). Epub 2024/01/04.
15. Chai, M. et al. Molecular mechanism of the protective effects of M2 microglia on neurons: a review focused on exosomes and secretory proteins. *Neurochem. Res.* **47** (12), 3556–3564. https://doi.org/10.1007/s11064-022-03760-4 (2022). Epub 2022/10/13.
16. Wan, T., Huang, Y., Gao, X., Wu, W. & Guo, W. Microglia polarization: a novel target of exosome for stroke treatment. *Front. Cell. Dev. Biol.* **10**, 842320. https://doi.org/10.3389/fcell.2022.842320 (2022). Epub 2022/04/01.
17. Xu, B. et al. Inhibition of PDE4 protects neurons against oxygen-glucose deprivation-induced endoplasmic reticulum stress through activation of the Nrf-2/HO-1 pathway. *Redox Biol.* **28**, 101342. https://doi.org/10.1016/j.redox.2019.101342 (2020). Epub 2019/10/23.
18. Xu, B. et al. Roflumilast prevents ischemic stroke-induced neuronal damage by restricting GSK3beta-mediated oxidative stress and IRE1alpha/TRAF2/JNK pathway. *Free Radic Biol. Med.* **163**, 281–296. https://doi.org/10.1016/j.freeradbiomed.2020.12.018 (2021). Epub 2020/12/29.
19. Chen, K. et al. Inhibition of phosphodiesterase 4 suppresses neuronal ferroptosis after cerebral ischemia/reperfusion. *Mol. Neurobiol.* **62** (3), 3376–3395. https://doi.org/10.1007/s12035-024-04495-9 (2025). Epub 2024/09/17 21:47.
20. Yu, X., Wang, S., Wang, X., Li, Y. & Dai, Z. Melatonin improves stroke by inhibiting autophagy-dependent ferroptosis mediated by NCOA4 binding to FTH1. *Exp. Neurol.* **379**, 114868. https://doi.org/10.1016/j.expneurol.2024.114868 (2024). Epub 2024/06/21.
21. Gu, H., Chen, Q. & Li, J. The MiR-101/EZH2 negative feedback signaling drives oxygen-glucose deprivation/reperfusion-induced injury by activating the MAPK14 signaling pathway in SH-SY5Y cells. *Acta Biochim. Pol.* **69** (2), 437–446. https://doi.org/10.18388/abp.2020_5921 (2022). Epub 2022/05/27.
22. Gu, H., Li, J. & Zhang, R. Melatonin upregulates DNA-PKcs to suppress apoptosis of human umbilical vein endothelial cells via inhibiting miR-101 under H(2)O(2)-induced oxidative stress. *Mol. Cell. Biochem.* **476** (2), 1283–1292. https://doi.org/10.1007/s11010-020-03991-5 (2021). Epub 2020/11/24.
23. Wang, G. et al. Itaconate promotes mitophagy to inhibit neuronal ferroptosis after subarachnoid hemorrhage. *Apoptosis* **30** (3–4), 991–1004. https://doi.org/10.1007/s10495-025-02077-1 (2025). Epub 2025/02/10.
24. Zhang, L., Lin, Y., Bai, W., Sun, L. & Tian, M. Human umbilical cord mesenchymal stem cell-derived exosome suppresses programmed cell death in traumatic brain injury via PINK1/Parkin-mediated mitophagy. *CNS Neurosci. Ther.* **29** (8), 2236–2258. https://doi.org/10.1111/cns.14159 (2023). Epub 2023/03/09.
25. Cai, Y. et al. FUNDC1-dependent mitophagy induced by tPA protects neurons against cerebral ischemia-reperfusion injury. *Redox Biol.* **38**, 101792. https://doi.org/10.1016/j.redox.2020.101792 (2021). Epub 2020/11/20.
26. Tang, T. et al. Src Inhibition rescues FUNDC1-mediated neuronal mitophagy in ischaemic stroke. *Stroke Vasc Neurol.* **9** (4), 367–379. https://doi.org/10.1136/svn-2023-002606 (2024). Epub 2023/10/05.
27. Ge, Q. et al. Xanthohumol regulates mitophagy in osteosarcoma cells via AMPK-ULK1-FUNDC1 signaling pathway. *Phytother Res.* https://doi.org/10.1002/ptr.8468 (2025). Epub 2025/04/07.
28. Yang, K. et al. NTRK1 knockdown induces mouse cognitive impairment and hippocampal neuronal damage through mitophagy suppression via inactivating the AMPK/ULK1/FUNDC1 pathway. *Cell. Death Discov.* **9** (1), 404. https://doi.org/10.1038/s41420-023-01685-7 (2023). Epub 2023/11/01.
29. Zheng, J. et al. Mechanisms of ferroptosis in hypoxic-ischemic brain damage in neonatal rats. *Exp. Neurol.* **372**, 114641. https://doi.org/10.1016/j.expneurol.2023.114641 (2024). Epub 2023/12/09.
30. Lin, F. et al. Mesenchymal stem cells protect against ferroptosis via exosome-mediated stabilization of SLC7A11 in acute liver injury. *Cell. Death Dis.* **13** (3), 271. https://doi.org/10.1038/s41419-022-04708-w (2022). Epub 2022/03/30.
31. Qi, R. et al. Cancer-associated fibroblasts suppress ferroptosis and induce gemcitabine resistance in pancreatic cancer cells by secreting exosome-derived ACSL4-targeting MiRNAs. *Drug Resist. Updat.* **68**, 100960. https://doi.org/10.1016/j.drup.2023.100960 (2023). Epub 2023/04/02.
32. Jiang, M. et al. Exosome-mediated miR-144-3p promotes ferroptosis to inhibit osteosarcoma proliferation, migration, and invasion through regulating ZEB1. *Mol. Cancer.* **22** (1), 113. https://doi.org/10.1186/s12943-023-01804-z (2023). Epub 2023/07/18.
33. Xie, K., Mo, Y., Yue, E., Shi, N. & Liu, K. Exosomes derived from M2-type microglia ameliorate oxygen-glucose deprivation/reoxygenation-induced HT22 cell injury by regulating miR-124-3p/NCOA4-mediated ferroptosis. *Heliyon* **9** (7), e17592. https://doi.org/10.1016/j.heliyon.2023.e17592 (2023). Epub 2023/07/10.
34. Picca, A., Faitg, J., Auwerx, J., Ferrucci, L. & D'Amico, D. Mitophagy in human health, ageing and disease. *Nat. Metab.* **5** (12), 2047–2061. https://doi.org/10.1038/s42255-023-00930-8 (2023). Epub 2023/12/01.
35. Wang, S. et al. The mitophagy pathway and its implications in human diseases. *Signal. Transduct. Target. Ther.* **8** (1), 304. https://doi.org/10.1038/s41392-023-01503-7 (2023). Epub 2023/08/16.
36. Lu, Y. et al. Cellular mitophagy: mechanism, roles in diseases and small molecule pharmacological regulation. *Theranostics* **13** (2), 736–766. https://doi.org/10.7150/thno.79876 (2023). Epub 2023/01/13.
37. Xu, B. T. et al. Mitofusin-2 mediates cannabidiol-induced neuroprotection against cerebral ischemia in rats. *Acta Pharmacol. Sin.* **44** (3), 499–512. https://doi.org/10.1038/s41401-022-01004-3 (2023). Epub 2022/10/14.
38. Zhang, X., Li, G., Chen, H., Nie, X. W. & Bian, J. S. Targeting NKAalpha1 to treat Parkinson's disease through Inhibition of mitophagy-dependent ferroptosis. *Free Radic Biol. Med.* **218**, 190–204. https://doi.org/10.1016/j.freeradbiomed.2024.04.002 (2024). Epub 2024/04/05.
39. Wang, Y. et al. Anti-ferroptosis exosomes engineered for targeting M2 microglia to improve neurological function in ischemic stroke. *J. Nanobiotechnol.* **22** (1), 291. https://doi.org/10.1186/s12951-024-02560-y (2024). Epub 2024/05/28.
40. Jin, Z. et al. Curcumin exerts chondroprotective effects against osteoarthritis by promoting AMPK/PINK1/Parkin-mediated mitophagy. *Biomed. Pharmacother.* **151**, 113092. https://doi.org/10.1016/j.biopha.2022.113092 (2022). Epub 2022/05/14.
41. Chu, C. et al. Neutrophil extracellular traps drive intestinal microvascular endothelial ferroptosis by impairing Fundc1-dependent mitophagy. *Redox Biol.* **67**, 102906. https://doi.org/10.1016/j.redox.2023.102906 (2023). PubMed PMID: 37812880; PubMed Central PMCID: PMCPMC10579540. Epub 2023/10/10.
42. Peng, H. et al. Ablation of FUNDC1-dependent mitophagy renders myocardium resistant to paraquat-induced ferroptosis and contractile dysfunction. *Biochim. Biophys. Acta Mol. Basis Dis.* **1868** (9), 166448. https://doi.org/10.1016/j.bbadis.2022.166448 (2022). Epub 2022/05/23.
43. Iorio, R., Celenza, G., & Petricca, S. Mitophagy: molecular mechanisms, new concepts on Parkin activation and the emerging role of AMPK/ULK1 axis. Cells **11**(1) (2021). https://doi.org/10.3390/cells11010030 (2021). PubMed PMID: 35011593; PubMed Central PMCID: PMCPMC8750607.
44. Ren, Y. et al. Lycium barbarum polysaccharide mitigates high-fat-diet-induced skeletal muscle atrophy by promoting AMPK/PINK1/Parkin-mediated mitophagy. *Int. J. Biol. Macromol.* **301**, 140488. https://doi.org/10.1016/j.ijbiomac.2025.140488 (2025). Epub 2025/02/01 20:42.

45. Wang, T. et al. Cadmium induces mitophagy via AMP-activated protein kinases activation in a PINK1/Parkin-dependent manner in PC12 cells. *Cell. Prolif.* **53** (6), e12817. https://doi.org/10.1111/cpr.12817 (2020). Epub 2020/05/13.
46. Liu, X. et al. Microglia-derived Exosomal circZNRF1 alleviates paraquat-induced neuronal cell damage via miR-17-5p. *Ecotoxicol. Environ. Saf.* **263**, 115356. https://doi.org/10.1016/j.ecoenv.2023.115356 (2023). Epub 2023/08/18.
47. Jiang, Y. et al. Glioblastoma-associated microglia-derived Exosomal circKIF18A promotes angiogenesis by targeting FOXC2. *Oncogene* **41** (26), 3461–3473. https://doi.org/10.1038/s41388-022-02360-4 (2022). Epub 2022/06/01.
48. Jiang, L., Li, H., Fan, Z., Zhao, R. & Xia, Z. Circular RNA expression profiles in neonatal rats following hypoxic-ischemic brain damage. *Int. J. Mol. Med.* **43** (4), 1699–1708. https://doi.org/10.3892/ijmm.2019.4111 (2019). Epub 2019/03/01.
49. Dong, X. et al. Expression profile of circular RNAs in the peripheral blood of neonates with hypoxic–ischemic encephalopathy. *Mol. Med. Rep.* **22** (1), 87–96. https://doi.org/10.3892/mmr.2020.11091 (2020). Epub 2020/05/30.

Author contributions
Hao Gu supervised the study and revised the manuscript. Jian Li wrote the manuscript and analyzed the experimental data. Jian Li and Qing Chen performed the experiments. All authors read and approved the final manuscript.

Funding
The authors declare that no funds, grants, or other support were received during the preparation of this manuscript.

Declarations

Competing interests
The authors declare no competing interests.

Ethics approval
None.

Consent to participate
None.

Consent to publish
None.

Additional information
Supplementary Information The online version contains supplementary material available at https://doi.org/10.1038/s41598-025-03091-8.

Correspondence and requests for materials should be addressed to H.G.

Reprints and permissions information is available at www.nature.com/reprints.

Publisher's note Springer Nature remains neutral with regard to jurisdictional claims in published maps and institutional affiliations.